

Subtle lattice distortion-driven phase transitions in layered ACu_4As_2(A=Eu, Sr)

Yong Nie(聂勇), Zheng Chen(陈正), Ming Mei(梅明), Yuan-Yuan Wang(王园园), Jia-Ting Wu(吴嘉挺), Jia-Liang Jiang(蒋佳良), Wen-Hai Song(宋文海), Wei Ning(宁伟), Zhao-Sheng Wang(王钊胜), Xiang-De Zhu(朱相德), and Ming-Liang Tian(田明亮)

Citation: Chin. Phys. B, 2023, 32 (**10**): 106102. DOI: 10.1088/1674-1056/acd36b

Journal homepage: http://cpb.iphy.ac.cn; http://iopscience.iop.org/cpb

What follows is a list of articles you may be interested in

Characterization of structural transitions and lattice dynamics of hybrid organic-inorganic perovskite $CH_3NH_3PbI_3$

Feng Jin(金峰), Jian-Ting Ji(籍建葶), Chao Xie(谢超), Yi-Meng Wang(王艺朦), Shu-Na He(贺淑娜), Lei Zhang(张磊), Zhao-Rong Yang(杨昭荣), Feng Yan(严锋), Qing-Ming Zhang(张清明)

Chin. Phys. B, 2019, 28 (**7**): 076102. DOI: 10.1088/1674-1056/28/7/076102

Size effect in the melting and freezing behaviors of Al/Ti core-shell nanoparticles using molecular dynamics simulations

Jin-Ping Zhang(张金平), Yang-Yang Zhang(张洋洋), Er-Ping Wang(王二萍), Cui-Ming Tang (唐翠明), Xin-Lu Cheng(程新路), Qiu-Hui Zhang(张秋慧)

Chin. Phys. B, 2016, 25 (**3**): 036102. DOI: 10.1088/1674-1056/25/3/036102

New crystal structure and physical properties of TcB from first-principles calculations

Zhang Gang-Tai (张刚台), Bai Ting-Ting (白婷婷), Yan Hai-Yan (闫海燕), Zhao Ya-Ru (赵亚儒)

Chin. Phys. B, 2015, 24 (**10**): 106104. DOI: 10.1088/1674-1056/24/10/106104

First-principles calculations of structural, electronic, and thermodynamic properties of $ZnO_{1-x}S_x$ alloys

Muhammad Zafar, Shabbir Ahmed, M. Shakil, M. A. Choudhary

Chin. Phys. B, 2014, 23 (**10**): 106108. DOI: 10.1088/1674-1056/23/10/106108

Structures and physical properties of R_2TX_3 compounds

Pan Zhi-Yan (潘志艳), Cao Chong-De (曹崇德), Bai Xiao-Jun (白晓军), Song Rui-Bo (宋瑞波), Zheng Jian-Bang (郑建邦), Duan Li-Bing (段利兵)

Chin. Phys. B, 2013, 22 (**5**): 056102. DOI: 10.1088/1674-1056/22/5/056102

Subtle lattice distortion-driven phase transitions in layered ACu_4As_2 (A = Eu, Sr)

Yong Nie(聂勇)[1,2], Zheng Chen(陈正)[1], Ming Mei(梅明)[1,2], Yuan-Yuan Wang(王园园)[1,2], Jia-Ting Wu(吴嘉挺)[1,2], Jia-Liang Jiang(蒋佳良)[1,2], Wen-Hai Song(宋文海)[3], Wei Ning(宁伟)[1,†], Zhao-Sheng Wang(王钊胜)[1], Xiang-De Zhu(朱相德)[1,‡], and Ming-Liang Tian(田明亮)[1,4,§]

[1] *Anhui Province Key Laboratory of Condensed Matter Physics at Extreme Conditions, High Magnetic Field Laboratory, Hefei Institutes of Physical Science (HFIPS), Chinese Academy of Sciences, Hefei* 230031, *China*

[2] *Department of Physics, University of Science and Technology of China, Hefei* 230026, *China*

[3] *Key Laboratory of Materials Physics, Institute of Solid State Physics, HFIPS, Chinese Academy of Sciences, Hefei* 230031, *China*

[4] *School of Physics, Anhui University, Hefei* 230601, *China*

(Received 5 April 2023; revised manuscript received 5 April 2023; accepted manuscript online 9 May 2023)

The compounds composed of transition metal cations and pnictide anions provide a rich platform for studying novel physical phenomena. Here we report on the observation of a phase transition at ∼ 70 K and 145 K in layered compound $EuCu_4As_2$ and $SrCu_4As_2$, respectively. from both the transport and heat capacity. The thermal expansion measurements show that the variation of the lattice parameters ($\Delta L_b/L_{ab}$) around T_P is much less than that for a typical crystalline phase transition. Our experimental results reveal that the transition in $EuCu_4As_2$ and $SrCu_4As_2$ should be driven by subtle structural-distortion.

Keywords: thermal expansion, specific heat, lattice-distortion

PACS: 61.66.–f, 65.40.Ba, 65.60.+a **DOI:** 10.1088/1674-1056/acd36b

1. Introduction

The compounds composed of transition metal cations and pnictide anions provide a rich platform for studying novel physical phenomena and various phase transitions, such as structural phase transition,[1] superconductivity,[2] magnetism,[3,4] and charge density wave (CDW) order.[5,6] For example, in $BaAg_2As_2$, an anomalous resistivity peak was observed at 150 K which derives from a structural distortion with the in-plane distortion without CDW and band reconstruction.[7] In the doped $BaFe_2As_2$, high temperature superconducting phase occurred in the vicinity of a collinear antiferromagnetic order and a tetragonal–orthorhombic structural distortion related to orbital/spin order.[8–10] Meanwhile, anomalous specific heat and electric transport were reported to be caused by a pure lattice-driven distortion in $BaNi_2As_2$,[11] so were the CDW-order-driven distortions in $BaPt_2As_2$ and $SrPt_2As_2$.[5,6] Recently, it has been reported that $SrAg_4As_2$ and $EuAg_4As_2$ exhibit anomalous resistivity at 110 K and 120 K.[12,13] In $EuAg_4As_2$, an anomalous resistivity transition at ∼ 120 K was regarded as a first-order structural transition, which is accompanied with a superlattice, which is verified by the single-crystal x-ray precession images below 120 K.[13] Like $EuAg_4As_2$, $EuCu_4As_2$ also displays an anomalous resistivity with a hysteresis at 75 K associated with structural distortion.[14] These findings suggest that further investigation of arsenides will be able to discover more exotic phenomena, which contributes to the study in this area.

In this work, we report on a study of two arsenides ACu_4As_2 (A = Eu and Sr) combined, by the measurements of electric transport, magnetization, heat capacity, transmission electron microscope (TEM), and thermal expansion. These two compounds were synthesized as early as decades ago. However, their physical properties have not been well studied yet. Our transport and heat capacity measurements show a transition at $T_P \sim 70$ K in $EuCu_4As_2$ and at $T_P \sim 145$ K in $SrCu_4As_2$. Thermal expansion reveals a subtle lattice parameter variation near T_P while the structural characterization of TEM shows no structure phase transition nor CDW below and above T_P. These results are in sharp contrast to the previous observations of $EuAg_4As_2$ and $EuCu_4As_2$. Our experimental data suggest that this transition is a nonmagnetic transition and relates to lattice distortion, which provides a clue to comprehending the transitions in $EuCu_4As_2$ and $SrCu_4As_2$.

2. Method

The crystals of $EuCu_4As_2$ and $SrCu_4As_2$ were synthesized by using Bi flux method. The molar ratio of elements was Eu shots (3N purity)/Sr shot (3N purity): Cu plates (4N purity): As shots (4N purity): Bi shots (5N purity) = 1:4:2:8. Oxide layer of Eu/Sr shots was scraped off from the surface.

†Corresponding author. E-mail: ningwei@hmfl.ac.cn
‡Corresponding author. E-mail: xdzhu@hmfl.ac.cn
§Corresponding author. E-mail: mltian@hmfl.ac.cn

© 2023 Chinese Physical Society and IOP Publishing Ltd

The mixture agents in the alumina crucible were sealed into a quartz tube under high vacuum. The furnace was heated to 950 °C and held for 3 days, then slowly cooled to 680 °C taking a week. The flux was removed by quick centrifugation. Several crystals each with a size of 2 mm×3 mm, were obtained, and the optical photographs of $EuCu_4As_2$ and $SrCu_4As_2$ are shown in the inset of Figs. 1(b) and 1(c), respectively.

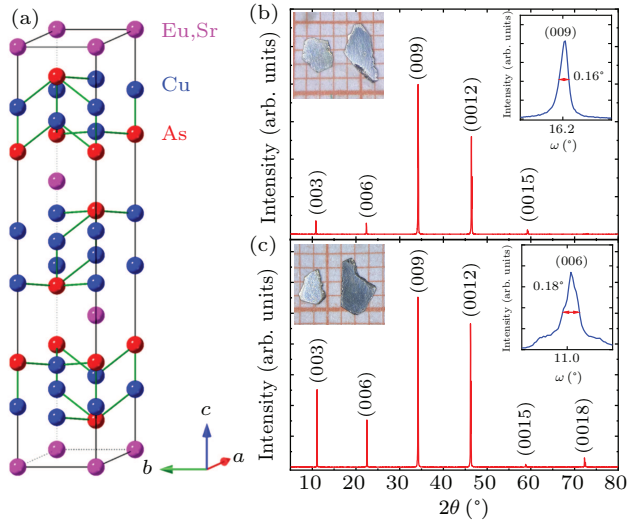


Fig. 1. (a) Crystal structural unit cell of ACu_4As_2 (A = Eu and Sr). XRD patterns of single crystal for (b) $EuCu_4As_2$ and (c) $SrCu_4As_2$, with the left insets showing optical images of several typical single crystals, and the right insets referring to the rocking curve at (009) peak of $EuCu_4As_2$ and (006) peak of $SrCu_4As_2$, respectively.

The compositions and stoichiometry of crystals were determined by energy dispersive spectrometer (EDS) equipped on SEM/FIB dual beam system (Helios nanolab600i, FEI Inc.). The x-ray diffraction (XRD) patterns were measured by Rigaku-TTR3 x-ray diffractometer using Cu-$K\alpha$ radiation. The magnetization was measured with a magnetic property measurement system (MPMS, QD Inc.). Resistivity and specific heat capacity measurements were performed on physical properties measurement system (PPMS-14T, QD Inc.). Selected area electron diffraction patterns were obtained by Talos F200X equipped with a liquid–nitrogen-cooled holder. Thermal expansion measurements in ab plane and along c axis were done by using home-made strain gauge[15] and capacitance dilatometer,[16] respectively.

3. Results and discussion

The layered compound ACu_4As_2 is iso-structural to $EuAg_4As_2$ and $SrAg_4As_2$ with the space group of $R\bar{3}m$ in rhombohedral $CaCu_4P_2$ structure[17] as illustrated in Fig. 1(a). Eu ions (Sr ions) are located between Cu_2As layers. The XRD patterns with crystalline indices (00l) are shown in Figs. 1(b) and 1(c) for $EuCu_4As_2$ and $SrCu_4As_2$, respectively. As shown in the inset of Figs. 1(b) and 1(c), the values of full width at half maximum (FWHM) of rocking curves are as low as 0.16° and 0.18° at the peak of (009) and (006), respectively, implying that these as-grown single crystals are of high quality.

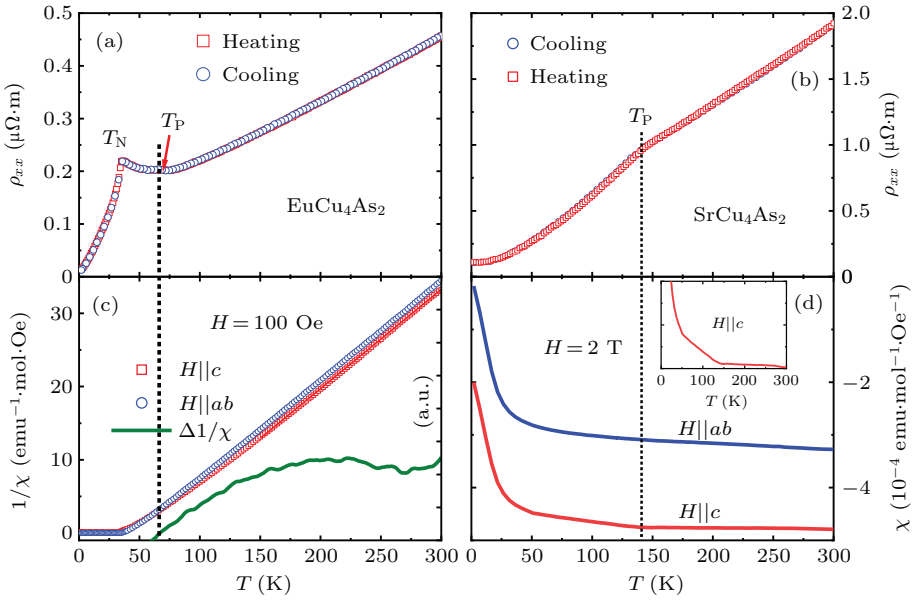


Fig. 2. Curves of temperature-dependent in-plane resistivity of (a) $EuCu_4As_2$ and (b) $SrCu_4As_2$ under heating (red line) and cooling (blue line) cycling at zero magnetic field, respectively. (c) Temperature-dependent reciprocal of susceptibility ($1/\chi$–T) measurement for $H \parallel c$ and $H \parallel ab$; difference in reciprocal of susceptibility between $H \parallel c$ and $H \parallel ab$ ($\Delta 1/\chi$) (olive line) for $EuCu_4As_2$ at $H = 100$ Oe (1 Oe = 79.5775 A·m^{-1}). (d) Temperature-dependent susceptibility for $H \parallel c$ and $H \parallel ab$ for $SrCu_4As_2$ at $H = 2$ T, with inset showing magnified part of $H \parallel c$ curve.

Figure 2(a) shows temperature-dependent resistivity of $EuCu_4As_2$. It suggests a metallic behavior in both heating cycle and cooling cycle. An hump at $T_P \sim 70$ K with no hysteresis and a peak at $T_N \sim 35$ K can be observed. The peak at T_N originates from ferromagnetic transition[14] and the hump at T_P is consistent with the bifurcation point of the $1/\chi$–T curves for $H \parallel ab$ and $H \parallel c$ as shown in Fig. 2(c). The $\Delta 1/\chi$ ($\Delta 1/\chi = 1/\chi_{ab} - 1/\chi_c$) curve (olive line) is plotted to observe

the difference of reciprocal of susceptibility between $H \parallel c$ and $H \parallel ab$ clearly. The anisotropic effective susceptibilities for $EuCu_4As_2$ at T_P are also observed in other systems, which is considered to stem from the crystal fields change.[18,19] Figure 2(b) displays the curves of temperature-dependent resistivity measured in both cooling and heating cycles for $SrCu_4As_2$, where a typical metallic behavior with a hump at $T_P \sim 145$ K but no hysteresis can be observed in the ρ_{xx}–T curves. Figure 2(d) exhibits the temperature-dependence of susceptibilities (χ–T) for $H \parallel ab$ and $H \parallel c$ at $H = 2$ T. A clear kink superimposed on the paramagnetic background is observed near T_P in the direction of $H \parallel c$. The inset shows part of of χ–T for $H \parallel c$. It is clear that the hump at T_P is unrelated to the magnetic moment of Eu ions as seen by comparing the results of electric transport and magnetization between $EuCu_4As_2$ and $SrCu_4As_2$.

In order to figure out the origin of the anomalous hump in ρ_{xx}–T curve at $T_P \sim 70$ K in $EuCu_4As_2$ and 145 K in $SrCu_4As_2$, temperature-dependent heat capacity (C_P) measurements at different magnetic fields in a temperature range from 2 K to 200 K are carried out as shown in Figs. 3(a) and 3(b). A peak at T_N and a hump at T_P can be identified from zero field heat capacity (green) for $EuCu_4As_2$. The hump at T_P remains unchanged under different magnetic fields while the peak at T_N gradually moves to higher temperature with the increase of magnetic field, indicating the underlying ferromagnetic transition as shown in the inset with a zoom-in near T_N. Like the scenario in $EuCu_4As_2$, a magnetic field independent hump can be observed in $SrCu_4As_2$. These results clearly reveal that the hump at T_P originates from a thermodynamic second order phase transition with a non-magnetic nature.

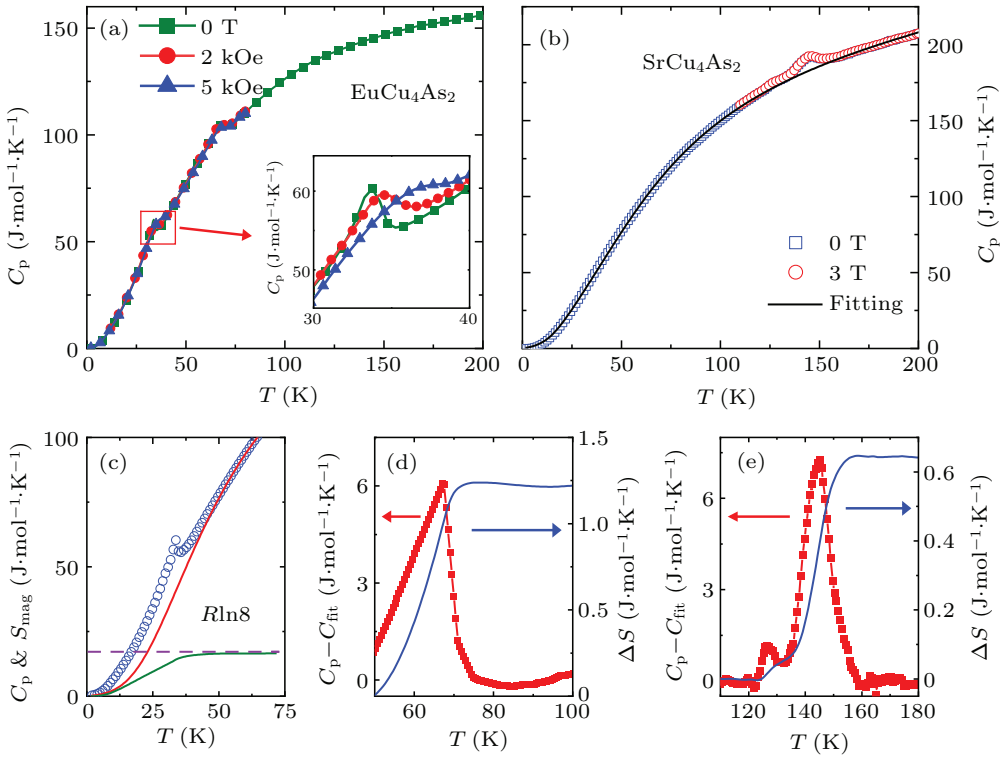


Fig. 3. (a) Heat capacity measurements of $EuCu_4As_2$ from 2 K to 200 K at $H = 0$ T, 2 kOe, and 5 kOe, with inset showing zoom-in around 35 K. (b) Heat capacity measurements of $SrCu_4As_2$ from 2 K to 200 K at $H = 0$ T and 3 T, with black linereferring to fitting line. (c) Fitting zero magnetic field heat capacity data (red solid line) from 70 K to 200 K after translating and magnifying part below 75 K and the magnetic contribution to the entropy (olive solid line) for $EuCu_4As_2$, with dashed line representing a reference guide line. Heat capacity in transition region corrected for the fitted background together with an estimate of the transition entropy obtained by integrating $(C_p–C_{fit})/T$ for (d) $EuCu_4As_2$ and (e) $SrCu_4As_2$, respectively.

The heat capacity data can be fitted by the expression $C = \gamma T + C_E + C_D$, where the first term γT on the right-hand side is the electron contribution, with γ being the Sommerfeld coefficient. C_E and C_D are the heat capacity furnished by the Einstein formula and Debye formula, respectively, specifically given by the following expressions:

$$C_E = 3n_E R \frac{y^2 e^y}{(e^y - 1)^2},$$

$$C_D = 9n_D R \left(\frac{T}{\theta_D}\right)^3 \int_0^{\theta_D} /T \frac{x^4 e^x}{(e^x - 1)^2}.$$

Here $x = \theta_D/T$, $y = \theta_E/T$, θ_D and θ_E are the Debye temperature and the Einstein temperature, respectively. The data ranging from 70 K to 200 K are translated up appropriately to eliminate the influence of the kink in $EuCu_4As_2$ as shown in Fig. 3(c). For $EuCu_4As_2$, C_E is not taken into account. The parameters $\gamma = 105.8$ mJ·mol^{-1}·K^{-1} and $\theta_D =$

209.24 K are obtained. The magnetic contribution $C_{\rm mag}$ in $EuCu_4As_2$ can be estimated by subtracting the electron and phonon contribution from the fitting result, and magnetic entropy from the magnetic ordering reaches a limiting value of 16.5 J·mol^{-1}·K^{-1} at 50 K, closing to the theoretical value of $R\ln 8$ ($R = 8.31$ J·mol^{-1}·K^{-1}). Transition entropy ΔS at $T_{\rm P}$ is estimated at 1.24 J·mol^{-1}·K^{-1}. For $SrCu_4As_2$, the data are fitted from 2 K to 115 K, as shown by the black line in Fig. 3(b). The parameters $\gamma = 242.2$ mJ·mol^{-1}·K^{-1}, $\theta_{\rm D} = 152$ K, and $\theta_{\rm E} = 258.5$ K are obtained. Transition entropy ΔS at $T_{\rm P}$ is estimated at 0.64 J·mol^{-1}·K^{-1}.

To figure out the origin of the phase transition near $T_{\rm P}$, the structural characterization from the SAED studies by using TEM technique is performed. Figures 4(a) and 4(c), and figures 4(b) and 4(d) show the SAED patterns with the electron incidence parallel to the [0001] and [10$\bar{1}$0] directions at 300 K and 100 K for $SrCu_4As_2$, respectively. The diffraction pattern below $T_{\rm P}$ is identical to that above $T_{\rm P}$. No noticeable change of crystal structures in space group occurs, indicating that the transition near $T_{\rm P}$ is irrelevant to structural phase transition or CDW transition. The SAED pattern of $EuCu_4As_2$ is absent, because the $T_{\rm P}$ below liquid nitrogen temperature is beyond the equipment limit. The experimental results of electric transport, magnetism, heat capacity, and SAED mentioned above demonstrate that the transition at $T_{\rm P}$ in our ACu_4As_2 does not trigger off any type of magnetic or structural transition nor space group changes.

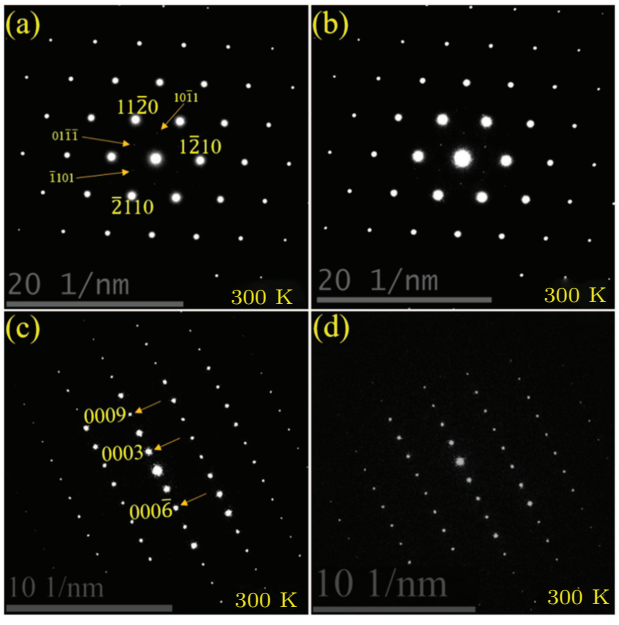


Fig. 4. SAED patterns of $SrCu_4As_2$ taken along zone axis [0001] at (a) 300 K and (b) 100 K, respectively. SAED patterns of $SrCu_4As_2$ taken along zone axis [10$\bar{1}$0] at (c) 300 K and (d) 100 K.

Figures 5(a) and 5(b) show the temperature-dependent thermal expansion ($\Delta L/L$) both in the *ab*-plane and along *c* axis for $EuCu_4As_2$ and $SrCu_4As_2$, respectively. A continuous drop of *c* axis about $\Delta L_c/L_c \sim 0.8‰$ and a continuous slight increase of *ab*-plane about $\Delta L_{ab}/L_{ab} \sim 0.196‰$ occur as temperature decreases from 74 K to 61 K in $EuCu_4As_2$. Similarly, a slight drop of *c* axis about $\Delta L_c/L_c \sim 1‰$ and a subtle increase of *ab*-plane about $\Delta L_{ab}/L_{ab} \sim 0.007‰$ are observed in $SrCu_4As_2$ when the temperature decreases from 160 K to 145 K. These subtle lattice parameter changes correspond to the $T_{\rm P}$ transition at 70 K in $EuCu_4As_2$ and 145 K in $SrCu_4As_2$ determined from the temperature-dependent resistivity and the susceptibility curves.

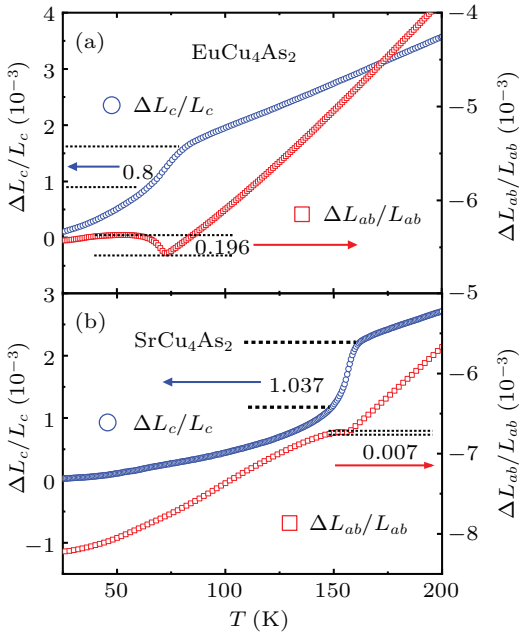


Fig. 5. Thermal expansion of lattice parameters in *ab* plane and along *c* axis in (a) $EuCu_4As_2$ and (b) $SrCu_4As_2$, respectively.

The transition of temperature-dependent resistivity has also been observed in several analogous compounds.[13,20,21] However, first-order specific heat peak and the emergence of superlattice peaks and hysteresis on ρ_{xx}–T curves are observed in $EuAg_4As_2$. While in $EuCu_4As_2$,[14] no hump on heat capacity and a small hysteresis on ρ_{xx}–T at $T_{\rm P}$ are observed. In both $EuAg_4As_2$ and $EuCu_4As_2$, this transition is attributed to the structural distortion. Furthermore, for $CaCu_4As_2$,[22] a kink at ~ 50 K with a hysteresis on ρ_{xx}–T is identified as a result of CDW transition. In our samples, the λ-type anomalous hump of heat capacity near $T_{\rm P}$ indicates that the $T_{\rm P}$-transition belongs to the second order-like thermodynamic phase transition. The conclusion of the second order transition can also be inferred from the result of subtle change of lattice parameters. This subtle lattice distortion is much smaller than a typical crystal structural transition with a lattice change on the order of $\sim 0.5\%$–1%.[23,24]

Additionally, similar phenomena have been observed in $Cd_2Re_2O_7$[25–27] and $LiOsO_3$,[28] including the anomalous kink in resistivity, λ-shaped anomalousness of heat capacity, and a kink in magnetization. This transition can be attributed to destruction of mirror symmetry caused by the average position displacement of Li ions in $LiOsO_3$ and Cd ions in

$Cd_2Re_2O_7$ measured by convergent beam electron diffraction (CBED). Therefore, the transition may originate from the displacement of Cu ions in $EuCu_4As_2$ and $SrCu_4As_2$. To further reveal the physical origin of the unique T_P transition, angle-resolved photoemission spectroscopy (ARPES), CBED, resonance inelastic x-ray scattering (RIXS) or scanning tunneling spectrum (STS) measurements are helpful in ascertaining the underlying physical origin of this intriguing transition.

4. Conclusions

In summary, $EuCu_4As_2$ and $SrCu_4As_2$ feature a transition at $T_P \sim 70$ K and 145 K, respectively. The origin of structural phase transition and CDW for this transition can be ruled out from the characterization of the SAED pattern under different temperatures. The thermal expansion measurements show that subtle lattice parameters change near T_P for both $EuCu_4As_2$ and $SrCu_4As_2$. The experimental observations suggest that the nonmagnetic transition at T_P should be related to lattice distortion and may originate from the displacement of Cu ions. Our results provide a platform for exploring the anomalous transitions.

Acknowledgements

Project supported by the National Key Research and Development Program of China (Grant No. 2021YFA1600201), the National Natural Science Foundation of China (Grant Nos. U19A2093, U2032214, U2032163, U1732274, 11904002, and 11874359), the Collaborative Innovation Program of Hefei Science Center, Chinese Academy of Sciences (CAS) (Grant No. 2019HSC-CIP 001), the Youth Innovation Promotion Association of CAS (Grant No. 2021117), the Natural Science Foundation of Anhui Province, China (Grant No. 1908085QA15), the Director Fund from the Hefei Institutes of Physical Science (HFIPS) (Grant No. YZJJQY202304), the Director Fund from the the Chinese Academy of Sciences and Hefei Institutes of Physical Science (CASHIPS), China (Grant No. E26MMG71131), and the High Magnetic Field Laboratory of Anhui Province, China.

References

[1] Huang Q, Qiu Y, Bao W, Green M A, Lynn J W, Gasparovic Y C, Wu T, Wu G and Chen X H 2008 *Phys. Rev. Lett.* **101** 257003
[2] Sefat A S, McGuire M A, Jin R, Sales B C, Mandrus D, Ronning F, Bauer E D and Mozharivskyj Y 2009 *Phys. Rev. B* **79** 094508
[3] Tan X, Tener Z P and Shatruk M 2018 *Accounts of Chemical Research* **51** 230
[4] Rotter M, Tegel M, Johrendt D, Schellenberg I, Hermes W and Pöttgen R 2008 *Phys. Rev. B* **78** 020503
[5] Jiang W B, Guo C Y, Weng Z F, Wang Y F, Chen Y H, Chen Y, Pang G M, Shang T, Lu X and Yuan H Q 2014 *J. Phys.: Condens. Matter* **27** 022202
[6] Kudo K, Nishikubo Y and Nohara M 2010 *J. Phys. Soc. Jpn.* **79** 123710
[7] Lou X, Xu H C, Wen C H P, Yu T L, Wei W Z, Yao Q, Song Y H, Emmanouilidou E, Shen B, Ni N, Dudin P, Huang Y B, Denlinger J, Sutarto R, Li W, Peng R and Feng D L 2020 *Phys. Rev. B* **101** 075123
[8] Fernandes R M, Chubukov A V and Schmalian J 2014 *Nat. Phys.* **10** 97
[9] Yi M, Lu D H, Analytis J G, Chu J H, Mo S K, He R H, Hashimoto M, Moore R G, Mazin I I, Singh D J, Hussain Z, Fisher I R and Shen Z X 2009 *Phys. Rev. B* **80** 174510
[10] Yang L X, Xie B P, Zhang Y, He C, Ge Q Q, Wang X F, Chen X H, Arita M, Jiang J, Shimada K, Taniguchi M, Vobornik I, Rossi G, Hu J P, Lu D H, Shen Z X, Lu Z Y and Feng D L 2010 *Phys. Rev. B* **82** 104519
[11] Zhou B, Xu M, Zhang Y, Xu G, He C, Yang L X, Chen F, Xie B P, Cui X Y, Arita M, Shimada K, Namatame H, Taniguchi M, Dai X and Feng D L 2011 *Phys. Rev. B* **83** 035110
[12] Shen B, Emmanouilidou E, Deng X, McCollam A, Xing J, Kotliar G, Coldea A I and Ni N 2018 *Phys. Rev. B* **98** 235130
[13] Shen B, Hu C, Cao H, Gui X, Emmanouilidou E, Xie W and Ni N 2020 *Phys. Rev. Mater.* **4** 064419
[14] Li L, Yang Z, Su Q, Yang J, Chen B, Du J, Wu C, Wang H and Fang M 2022 *J. Alloys Compd.* **916** 165460
[15] Luo X, Sun Y P, Lu W J, Zhu X B, Yang Z R and Song W H 2010 *Appl. Phys. Lett.* **96** 062506
[16] Kuchler R, Worl A, Gegenwart P, Berben M, Bryant B and Wiedmann S 2017 *Rev. Sci. Instrum.* **88** 083903
[17] Dünner J and Mewis A 1997 *Z. Anorg. Allg. Chem.* **623** 608
[18] Tovar M, Rao D, Barnett J, Oseroff S B, Thompson J D, Cheong S W, Fisk Z, Vier D C and Schultz S 1989 *Phys. Rev. B* **39** 2661
[19] Miyazawa M 2005 *J. Phys. Soc. Jpn.* **75** 014702
[20] Bud'ko S L, Xiang L, Hu C, Shen B, Ni N and Canfield P C 2020 *Phys. Rev. B* **101** 195112
[21] Zhu Q, Li L, Yang Z, Lou Z, Du J, Yang J, Chen B, Wang H and Fang M 2020 *Sci. China: Phys., Mech. Astron.* **64** 227011
[22] Sasmal S, Saini V, Ramakrishnan S, Dwari G, Maity B B, Bao J K, Mondal R, Tripathi V, van Smaalen S, Singh B and Thamizhavel A 2022 *Phys. Rev. Res.* **4** L012011
[23] Fernández-Díaz M T, Martínez J L, Alonso J M and Herrero E 1999 *Phys. Rev. B* **59** 1277
[24] Kuwahara H, Tomioka Y, Asamitsu A, Moritomo Y and Tokura Y 1995 *Science* **270** 961
[25] Tachibana M, Taira N, Kawaji H and Takayama-Muromachi E 2010 *Phys. Rev. B* **82** 054108
[26] Yamaura J and Hiroi Z 2002 *J. Phys. Soc. Jpn.* **71** 2598
[27] Hiroi Z, Yamaura J I, Muraoka Y and Hanawa M 2002 *J. Phys. Soc. Jpn.* **71** 1634
[28] Shi Y, Guo Y, Wang X, Princep A J, Khalyavin D, Manuel P, Michiue Y, Sato A, Tsuda K, Yu S, Arai M, Shirako Y, Akaogi M, Wang N, Yamaura K and Boothroyd A T 2013 *Nat. Mater.* **12** 1024